



# Effects of shell thickness on the electric field dependence of exciton recombination in CdSe/CdS core/shell quantum dots

CLARE E. ROWLAND,<sup>1</sup> MARC CURRIE,<sup>2</sup> KIMIHIRO SUSUMU,<sup>2,3</sup> EUNKEU OH,<sup>2,3</sup> GARY KUSHTO,<sup>2</sup> ALEXANDER L. EFROS,<sup>4</sup> ALAN H. HUSTON,<sup>2</sup> AND JAMES B. DELEHANTY<sup>5,\*</sup>

<sup>1</sup>National Research Council, Washington, DC 20036, USA

<sup>2</sup>Optical Sciences Division, Naval Research Laboratory, Code 5600, 4555 Overlook Ave. SW, Washington, D.C. 20375, USA

<sup>3</sup>Sotera Defense Solutions, Columbia, MD 21046, USA

<sup>4</sup>Materials Science and Technology Division, Naval Research Laboratory, Code 6300, 4555 Overlook Ave. SW, Washington, D.C., 20375, USA

<sup>5</sup>Center for Bio/Molecular Science and Engineering, Naval Research Laboratory, Code 6900, 4555 Overlook Ave. SW, Washington, D.C., 20375, USA

\*james.delehanty@nrl.navy.mil

**Abstract:** Here we examine the effects of shell thickness on the photophysical properties of CdSe/CdS core/shell quantum dots (QDs) in an electric field. Photoluminescence (PL) of QDs in an applied electric field is observed to decrease markedly with increasing shell thickness, with a thick-shelled (4.9 nm shell) sample exhibiting an order of magnitude greater PL suppression than a thin-shelled sample (1.25 nm shell) with the same core.

**OCIS codes:** (160.4236) Nanomaterials; (160.4670) Optical materials; (160.4760) Optical properties; (250.5230) Photoluminescence.

## References and links

1. J. C. Claussen, N. Hildebrandt, K. Susumu, M. G. Ancona, and I. L. Medintz, "Complex logic functions implemented with quantum dot bionanophotonic circuits," *ACS Appl. Mater. Interfaces* **6**(6), 3771–3778 (2014).
2. L. D. Field, J. B. Delehanty, Y. Chen, and I. L. Medintz, "Peptides for specifically targeting nanoparticles to cellular organelles: quo vadis?" *Acc. Chem. Res.* **48**(5), 1380–1390 (2015).
3. Y. P. Ho and K. W. Leong, "Quantum dot-based theranostics," *Nanoscale* **2**(1), 60–68 (2010).
4. S. M. Goodman, A. Siu, V. Singh, and P. Nagpal, "Long-range energy transfer in self-assembled quantum dot-DNA cascades," *Nanoscale* **7**(44), 18435–18440 (2015).
5. C. E. Rowland, C. W. Brown III, I. L. Medintz, and J. B. Delehanty, "Intracellular FRET-based probes: a review," *Methods Appl. Fluoresc.* **3**(4), 042006 (2015).
6. C. E. Rowland, J. B. Delehanty, C. L. Dwyer, and I. L. Medintz, "Growing applications for bioassembled resonance energy transfer cascades," *Mater. Today* (2016), doi:10.1016/j.mattod.2016.09.013.
7. K. E. Sapsford, W. R. Algar, L. Berti, K. B. Gemmill, B. J. Casey, E. Oh, M. H. Stewart, and I. L. Medintz, "Functionalizing nanoparticles with biological molecules: developing chemistries that facilitate nanotechnology," *Chem. Rev.* **113**(3), 1904–2074 (2013).
8. P. Zrazhevskiy, M. Sena, and X. Gao, "Designing multifunctional quantum dots for bioimaging, detection, and drug delivery," *Chem. Soc. Rev.* **39**(11), 4326–4354 (2010).
9. V. I. Klimov, "Spectral and dynamical properties of multiexcitons in semiconductor nanocrystals," *Annu. Rev. Phys. Chem.* **58**(1), 635–673 (2007).
10. A. Bhirde, J. Xie, M. Swierczewska, and X. Chen, "Nanoparticles for cell labeling," *Nanoscale* **3**(1), 142–153 (2011).
11. P. D. Howes, R. Chandrawati, and M. M. Stevens, "Colloidal nanoparticles as advanced biological sensors," *Science* **346**(6205), 1247390 (2014).
12. A. M. Dennis, W. J. Rhee, D. Sotto, S. N. Dublin, and G. Bao, "Quantum dot-fluorescent protein FRET probes for sensing intracellular pH," *ACS Nano* **6**(4), 2917–2924 (2012).
13. J. B. Delehanty, J. C. Breger, K. B. Gemmill, M. H. Stewart, and I. L. Medintz, "Controlling the actuation of therapeutic nanomaterials: enabling nanoparticle-mediated drug delivery," *Ther. Deliv.* **4**(11), 1411–1429 (2013).
14. V. Bagalkot, L. Zhang, E. Levy-Nissenbaum, S. Jon, P. W. Kantoff, R. Langer, and O. C. Farokhzad, "Quantum dot-aptamer conjugates for synchronous cancer imaging, therapy, and sensing of drug delivery based on bi-fluorescence resonance energy transfer," *Nano Lett.* **7**(10), 3065–3070 (2007).

15. C. E. Rowland, K. Susumu, M. H. Stewart, E. Oh, A. J. Mäkinen, T. J. O'Shaughnessy, G. Kushto, M. A. Wolak, J. S. Erickson, A. L. Efros, A. L. Huston, and J. B. Delehanty, "Electric field modulation of semiconductor quantum dot photoluminescence: insights into the design of robust voltage-sensitive cellular imaging probes," *Nano Lett.* **15**(10), 6848–6854 (2015).
16. C. E. Rowland, K. Susumu, M. H. Stewart, E. Oh, A. J. Mäkinen, T. J. O'Shaughnessy, G. Kushto, M. A. Wolak, J. S. Erickson, and A. L. Efros, "Imaging cellular membrane potential through ionization of quantum dots," *Proc. SPIE* **9722**, 97220 (2016).
17. A. Abbott, "Neuroscience: solving the brain," *Nature* **499**(7458), 272–274 (2013).
18. A. P. Alivisatos, A. M. Andrews, E. S. Boyden, M. Chun, G. M. Church, K. Deisseroth, J. P. Donoghue, S. E. Fraser, J. Lippincott-Schwartz, L. L. Looger, S. Masmanidis, P. L. McEuen, A. V. Nurmikko, H. Park, D. S. Peterka, C. Reid, M. L. Roukes, A. Scherer, M. Schnitzer, T. J. Sejnowski, K. L. Shepard, D. Tsao, G. Turrigiano, P. S. Weiss, C. Xu, R. Yuste, and X. Zhuang, "Nanotools for neuroscience and brain activity mapping," *ACS Nano* **7**(3), 1850–1866 (2013).
19. A. P. Alivisatos, M. Chun, G. M. Church, R. J. Greenspan, M. L. Roukes, and R. Yuste, "The brain activity map project and the challenge of functional connectomics," *Neuron* **74**(6), 970–974 (2012).
20. B. Sakmann and E. Neher, "Patch clamp techniques for studying ionic channels in excitable membranes," *Annu. Rev. Physiol.* **46**(1), 455–472 (1984).
21. M. E. Spira and A. Hai, "Multi-electrode array technologies for neuroscience and cardiology," *Nat. Nanotechnol.* **8**(2), 83–94 (2013).
22. T.-W. Chen, T. J. Wardill, Y. Sun, S. R. Pulver, S. L. Renninger, A. Baohan, E. R. Schreiter, R. A. Kerr, M. B. Orger, V. Jayaraman, L. L. Looger, K. Svoboda, and D. S. Kim, "Ultrasensitive fluorescent proteins for imaging neuronal activity," *Nature* **499**(7458), 295–300 (2013).
23. V. Tsytarev, L. D. Liao, K. V. Kong, Y. H. Liu, R. S. Erzurumlu, M. Olivo, and N. V. Thakor, "Recent progress in voltage-sensitive dye imaging for neuroscience," *J. Nanosci. Nanotechnol.* **14**(7), 4733–4744 (2014).
24. D. Bozyigit, O. Yarema, and V. Wood, "Origins of low quantum efficiencies in quantum dot LEDs," *Adv. Funct. Mater.* **23**(24), 3024–3029 (2013).
25. D. Bozyigit, V. Wood, Y. Shirasaki, and V. Bulovic, "Study of field driven electroluminescence in colloidal quantum dot solids," *J. Appl. Phys.* **111**(11), 113701 (2012).
26. K. Park, Z. Deutsch, J. J. Li, D. Oron, and S. Weiss, "Single molecule quantum-confined Stark effect measurements of semiconductor nanoparticles at room temperature," *ACS Nano* **6**(11), 10013–10023 (2012).
27. S. A. Empedocles and M. G. Bawendi, "Quantum-confined stark effect in single CdSe nanocrystallite quantum dots," *Science* **278**(5346), 2114–2117 (1997).
28. T. D. Krauss and L. E. Brus, "Electronic properties of single semiconductor nanocrystals: optical and electrostatic force microscopy measurements," *Mat. Sci. Eng. B-Solid* **69-70**, 289–294 (2000).
29. H. Huang, A. Dorn, G. P. Nair, V. Bulović, and M. G. Bawendi, "Bias-induced photoluminescence quenching of single colloidal quantum dots embedded in organic semiconductors," *Nano Lett.* **7**(12), 3781–3786 (2007).
30. C. A. Leatherdale, C. R. Kagan, N. Y. Morgan, S. A. Empedocles, M. A. Kastner, and M. G. Bawendi, "Photoconductivity in CdSe quantum dot solids," *Phys. Rev. B* **62**(4), 2669–2680 (2000).
31. A. P. Alivisatos, W. Gu, and C. Larabell, "Quantum dots as cellular probes," *Annu. Rev. Biomed. Eng.* **7**(1), 55–76 (2005).
32. R. Walters, R. P. Kraig, I. Medintz, J. B. Delehanty, M. H. Stewart, K. Susumu, A. L. Huston, P. E. Dawson, and G. Dawson, "Nanoparticle targeting to neurons in a rat hippocampal slice culture model," *ASN Neuro* **4**(6), 383–392 (2012).
33. R. Agarwal, M. S. Domowicz, N. B. Schwartz, J. Henry, I. Medintz, J. B. Delehanty, M. H. Stewart, K. Susumu, A. L. Huston, J. R. Deschamps, P. E. Dawson, V. Palomo, and G. Dawson, "Delivery and tracking of quantum dot peptide bioconjugates in an intact developing avian brain," *ACS Chem. Neurosci.* **6**(3), 494–504 (2015).
34. K. Boeneman, J. B. Delehanty, J. B. Blanco-Canosa, K. Susumu, M. H. Stewart, E. Oh, A. L. Huston, G. Dawson, S. Ingale, R. Walters, M. Domowicz, J. R. Deschamps, W. R. Algar, S. Dimaggio, J. Manono, C. M. Spillmann, D. Thompson, T. L. Jennings, P. E. Dawson, and I. L. Medintz, "Selecting improved peptidyl motifs for cytosolic delivery of disparate protein and nanoparticle materials," *ACS Nano* **7**(5), 3778–3796 (2013).
35. G. Gopalakrishnan, C. Danelon, P. Izewska, M. Prummer, P. Y. Bolinger, I. Geissbühler, D. Demurtas, J. Dubochet, and H. Vogel, "Multifunctional lipid/quantum dot hybrid nanocontainers for controlled targeting of live cells," *Angew. Chem. Int. Ed. Engl.* **45**(33), 5478–5483 (2006).
36. U. Resch-Genger, M. Grabolle, S. Cavaliere-Jaricot, R. Nitschke, and T. Nann, "Quantum dots versus organic dyes as fluorescent labels," *Nat. Methods* **5**(9), 763–775 (2008).
37. A. R. Clapp, T. Pons, I. L. Medintz, J. B. Delehanty, J. S. Melinger, T. Tiefenbrunn, P. E. Dawson, B. R. Fisher, B. O'Rourke, and H. Mattoussi, "Two-photon excitation of quantum dot-based fluorescence resonance energy transfer and its applications," *Adv. Mater.* **19**(15), 1921–1926 (2007).
38. I. L. Medintz and H. Mattoussi, "Quantum dot-based resonance energy transfer and its growing application in biology," *Phys. Chem. Chem. Phys.* **11**(1), 17–45 (2009).
39. A. R. Clapp, I. L. Medintz, and H. Mattoussi, "Förster resonance energy transfer investigations using quantum-dot fluorophores," *ChemPhysChem* **7**(1), 47–57 (2006).
40. D. R. Larson, W. R. Zipfel, R. M. Williams, S. W. Clark, M. P. Bruchez, F. W. Wise, and W. W. Webb, "Water-soluble quantum dots for multiphoton fluorescence imaging in vivo," *Science* **300**(5624), 1434–1436 (2003).

41. B. K. Andrásfalvy, G. L. Galiñanes, D. Huber, M. Barbic, J. J. Macklin, K. Susumu, J. B. Delehanty, A. L. Huston, J. K. Makara, and I. L. Medintz, "Quantum dot-based multiphoton fluorescent pipettes for targeted neuronal electrophysiology," *Nat. Methods* **11**(12), 1237–1241 (2014).
42. A. Shabaev, A. Rodina, and A. L. Efros, "Fine structure of the band-edge excitons and trions in CdSe/CdS core/shell nanocrystals," *Phys. Rev. B* **86**(20), 205311 (2012).
43. K. H. Schmidt, G. Medeiros-Ribeiro, and P. M. Petroff, "Photoluminescence of charged InAs self-assembled quantum dots," *Phys. Rev. B* **58**(7), 3597–3600 (1998).
44. B. A. Lewis and D. M. Engelman, "Lipid bilayer thickness varies linearly with acyl chain length in fluid phosphatidylcholine vesicles," *J. Mol. Biol.* **166**(2), 211–217 (1983).
45. L. Dong, A. Sugunan, J. Hu, S. Zhou, S. Li, S. Popov, M. S. Toprak, A. T. Friberg, and M. Muhammed, "Photoluminescence from quasi-type-II spherical CdSe-CdS core-shell quantum dots," *Appl. Opt.* **52**(1), 105–109 (2013).
46. L. P. Balet, S. A. Ivanov, A. Piryatinski, M. Achermann, and V. I. Klimov, "Inverted core/shell nanocrystals continuously tunable between Type-I and Type-II localization regimes," *Nano Lett.* **4**(8), 1485–1488 (2004).
47. J. D. Marshall and M. J. Schnitzer, "Optical strategies for sensing neuronal voltage using quantum dots and other semiconductor nanocrystals," *ACS Nano* **7**(5), 4601–4609 (2013).
48. D. Chen, F. Zhao, H. Qi, M. Rutherford, and X. Peng, "Bright and stable purple/blue emitting CdS/ZnS core/shell nanocrystals grown by thermal cycling using a single-source precursor," *Chem. Mater.* **22**(4), 1437–1444 (2010).

## 1. Introduction

The unique properties of nanomaterials (NMs) that arise from the controlled arrangement of atoms in materials synthesized on the nanoscale have enabled their implementation in fields as diverse as quantum encryption, light harvesting, and medical diagnosis and treatment [1–6]. In recent years, their use in biological applications has seen extraordinary expansion thanks in large part to a number of intrinsic attributes that make NMs well-suited for use in biological environments. These include the inherent small size of NMs and their accompanying size-dependent photophysical properties (in semiconductors), as well as the ability to controllably alter or "tune" their surface chemistry through functionalization and bioconjugation [7–9]. Applications of semiconductor quantum dots (QDs) have seen almost exponential growth in *in vitro* and *in vivo* labeling and imaging [2,10], sensing [11,12], and drug delivery and actuation [5,13,14]. Within this field, our group recently demonstrated that the intrinsic sensitivity of the photoluminescence (PL) of QDs to an external electric field can be used to detect changes in the latter with millisecond temporal resolution, a property with direct relevance to real-time imaging of neuronal cell action potentials and, more generally, to the high-throughput imaging of the activity of electrically excitable cells [15,16].

Brain mapping endeavors, including the United States' BRAIN Initiative and its European counterpart, the Human Brain Project, seek to map the neuronal "connectome" of the human brain: the functional interconnections of the tens of billions of neurons that comprise the brain [17–19]. A desired goal of this daunting challenge is the combined simultaneous visualization/recording of the activity of thousands of neurons while retaining the ability to resolve the activity of a single neuron with spatiotemporal resolution. While current techniques exist that can operate with single-cell resolution (*e.g.*, patch clamp) or with much broader field of view (*e.g.*, electrode arrays), no single technique or material currently offers the desired high-throughput with single cell resolution [20,21]. Optical imaging techniques offer a potential avenue for attaining both, but currently available fluorophores come with their own limitations. Fluorescent proteins such as GCaMP6, the genetic fusion of green fluorescent protein to a  $\text{Ca}^{2+}$ -binding moiety, requires cellular transfection or the generation of transgenic animals and measures  $\text{Ca}^{2+}$  influx triggered by the action potential rather than directly measuring membrane voltage [22]. Organic voltage-sensitive dyes exhibit only modest changes in PL intensity in response to electric fields, are susceptible to photobleaching, and can be toxic [23]. QDs, with their intrinsic susceptibility to electric fields [24–30], superior photostability [31], low cytotoxicity [32,33], and other properties that have made them powerful tools in bio-imaging [34–41] have emerged as a potential powerfully enabling material for imaging action potentials in large numbers of cells in realtime with exquisite spatiotemporal resolution.

In our previous research, we examined the effects of electric fields on the quenching of the PL of Type I and quasi-Type II core/shell QDs and observed substantially better electric field-driven PL attenuation in the quasi-Type II QDs as compared to Type I QDs. We attributed these differences in PL response between the two samples to the ability of the electric field to ionize the QDs, a process facilitated by the localization of charge carriers (electrons or holes) in the material's shell (in the case of quasi-Type II QDs) but impeded by the presence of a relatively insulating shell around an electron localized in the core (for Type I QDs). These results suggested, therefore, that efforts to increase QD PL susceptibility to electric fields should focus on QD structures in which the carriers are spatially separated. Such spatial separation of carriers is straight-forward in Type II core/thick shell structures but also occurs in Type I core/shell structures with small band offset for one of the carriers because the power of a quantum well created by a core with small radius is insufficient for carrier localization in the core [42]. This occurs, for example, in Type I CdSe/CdS core/shell QDs, in which the electron/hole separation should increase with the shell thickness.

## 2. Quantum dots for shell thickness-dependent PL response to electric field

In the present study we have synthesized CdSe/CdS core/shell QDs with a series of increasingly thicker CdS shells, referred to here as samples A-D (Fig. 1(a)), and have determined their PL response to an applied electric field (Fig. 1(b)). Full details of the synthesis and characterization of these QDs are available in the Appendices 1.1 and 1.2 (Table 1).

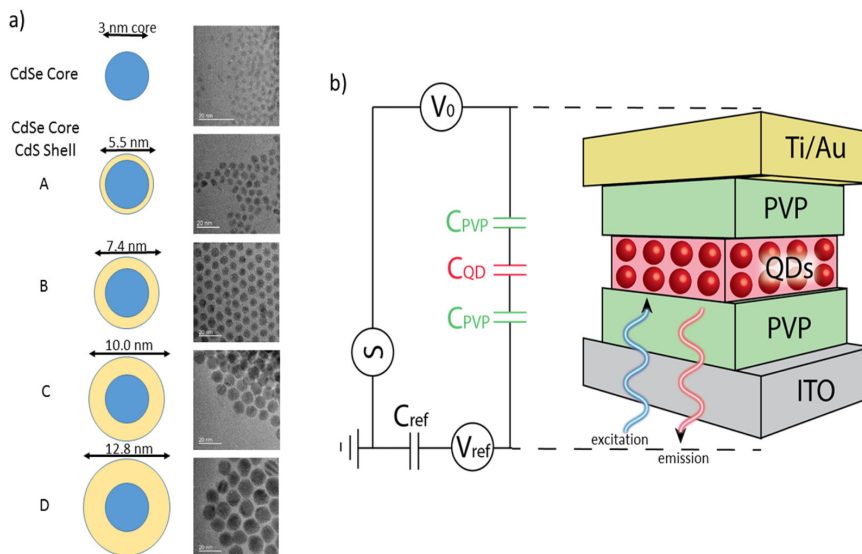


Fig. 1. (a) A single CdSe core size was coated with CdS shells of increasing thickness. QD diameter was determined by TEM. Scale bar in each is 20 nm. (b) A layer of QDs in PMMA was sandwiched between layers of PVP, which were in turn placed between two electrodes. The QDs were photoexcited and PL was collected through the transparent ITO electrode. This capacitive device was integrated into a Sawyer-Tower circuit, which allowed for the determination of the electric field experienced by the QDs. The samples were photoexcited using a 400 nm diode laser while being subjected to an electric field by passing a periodic square potential wave through the Sawyer-Tower circuit. Photoluminescence was collected by a fiber coupled microscope objective and dispersed *via* a grating onto a back thinned, UV enhanced CCD gated to integrate only when the sample reached the desired potential in order to generate spectrally-resolved data. See Appendix 1.3 for device fabrication.

The CdSe/CdS QDs were dispersed in poly(methyl methacrylate) and spin-coated between layers of poly(vinyl pyrrolidone) (PVP). The use of dielectric polymers in the

assembly ensured that our measurements reflected the application of an electric field to the QDs rather than the introduction of exogenous electrons, or charging, which is also known to have an effect on PL [43]. Spin-coating this dielectric “sandwich” over a transparent ITO electrode on a glass substrate and depositing a Ti/Au electrode on top completed the fabrication of the device that was then integrated into a Sawyer-Tower circuit, as shown in Fig. 1(b) (see also Appendix 1.4, Fig. 4, Table 2). An arbitrary waveform generator was then used to apply a potential to the circuit, and the potential drop over the device was measured. The electric field experienced by the QDs ( $E$ ) could then be calculated using the following equation (see Appendix 1.4 for derivation):

$$E = \frac{1}{d} [V_{ref} (2 \frac{C_{ref}}{C_{PVP}} + 1) - V_0], \quad (1)$$

where  $d$  is the thickness of the PMMA film containing the QDs,  $C_{PVP}$  is the capacitance of the PVP layers,  $C_{ref}$  is the capacitance of a reference capacitor,  $V_0$  is the applied voltage, and  $V_{ref}$  is the voltage measured between the device and the reference capacitor.

### 3. Effect of shell thickness on QD PL response to applied electric field

#### 3.1 Effect of electric field on QDs of varying shell thicknesses

As shown in Fig. 2, increased electric fields resulted in a decrease in PL intensity, a feature associated with the quantum-confined Stark effect and consistent with our previous observations [15, 16]. Examining QDs with shells of varying thickness, however, adds nuance to the observations. Sample A, with the thinnest shell (1.25 nm), displayed almost no drop in PL intensity (less than 10% decrease in PL from 0 MV/cm field to 3.3 MV/cm (Fig. 2(a))), while the sample with the thickest shell (4.9 nm), D, exhibited the most substantial change (25% decrease when 3.7 MV/cm field was applied (Fig. 2(b))). The two remaining samples with intermediary shell thicknesses exhibited responses that fell between the thinnest and thickest shell samples. The electric field-dependent PL intensity response was compared among samples by tracking the changes in peak intensity of QD emission with increasing field strength (Fig. 2(c)).

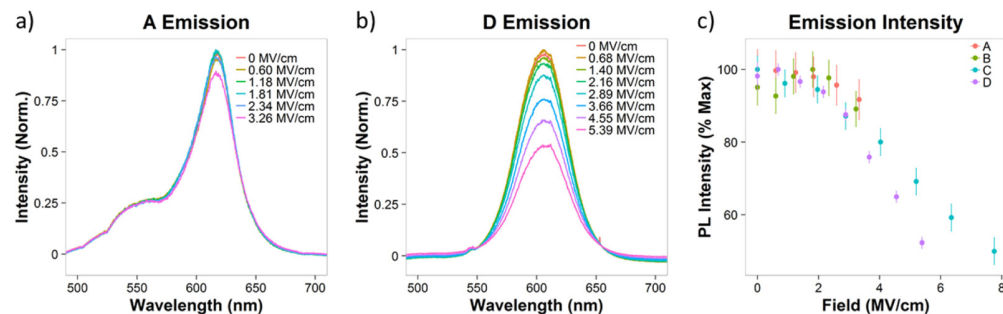


Fig. 2. (a) Sample A, a CdSe core with a thin (1.25 nm) CdS shell, exhibits only slight suppression of PL intensity upon application of an electric field. (b) Emission from Sample D, which possesses a thick (4.9 nm) CdS shell, shows significant susceptibility to the strength of an applied electric field. (c) Emission intensity from a series of cores with increasing shell thickness demonstrates a general trend of increasing electric field-driven PL suppression with increasing shell thickness. The error on the emission intensity data reflects the deviation between the as-collected data and the Gaussian-fitted data that was used to obtain the peaks' change in full width at half maximum.

For context, the total change in electric field felt across a cell's plasma membrane during an action potential is approximately 0.24 MV/cm (24 mV/nm) [44]. Because the membrane resting potential is negative ( $\sim 70$  mV) and the action potential crosses through zero field

(reaching a maximum of  $\sim +50$  mV), the maximum field strength experienced in the plasma membrane is lower still, around 0.14 MV/cm. Note that the PL responses of samples A and B, with their thinner shells, could only be measured using this experimental setup up to fields of  $\sim 3$  MV/cm before the field strength began to fluctuate in the device. It is worth noting that the thin shell of sample A means that it may not have the fully separated carriers that we suggest leads to enhanced PL suppression, as carrier overlap is greater in thinner-shelled CdSe/CdS QDs [45, 46]. The competition between thermo-population and the rate of radiative decay of the two lowest electron levels in these structures could also be the source of the two line structures in the PL. Neither the expected spectral broadening nor red-shifting of the emission maximum was able to be measured within the spectral resolution of the instrument. Although we observed evidence of these trends in other materials, it is unsurprising that these properties should be difficult to detect at ambient temperatures [15, 16]. Because changes in the spectral shape/breadth and central emission wavelength were minimal, we were able to examine the samples using a PMT, a method that allowed for more rapid data collection by integrating total emission and foregoing spectral resolution. This approach circumvented the low sample stability at elevated electric fields that was evident in samples A and B. By applying a sinusoidal electric field to the circuit at 10 Hz, the experiment could be completed quickly, and the instability in the electric field – evidenced by fluctuations in the voltage drop measured at  $V_{\text{ref}}$  – was no longer observed.

### 3.2 Effect of number of excitons and shell thickness on electric field-induced modulation of QD PL

In order to account for changes in the absorption profile of the QDs among the samples, we also adjusted the laser power and were thus able to excite the ensemble to generate an average of 0.01, 0.1, and 1 exciton per QD (Fig. 3). Using this approach, we confirmed the findings shown in Fig. 2 – that is, the degree of attenuation of the QD PL by an applied electric field correlates directly with the thickness of the shell, a trend that holds at both high (1 exciton/QD) and low (0.01 exciton/QD) excitation levels. At 0.1 exciton/QD, for example, the thickest-shelled sample (Sample D) is an order of magnitude more sensitive to field strengths of 2 MV/cm than the thinnest-shelled sample (Sample A), as shown in Fig. 3(a). Results obtained from sample D, with its relatively larger changes in PL intensity, suggest an additional possibility, namely that the QDs exhibit a greater sensitivity to electric fields at lower excitation levels (Fig. 3(b)). For the other samples, however, the signal/noise ratio obscured this information (Fig. 3(c)).

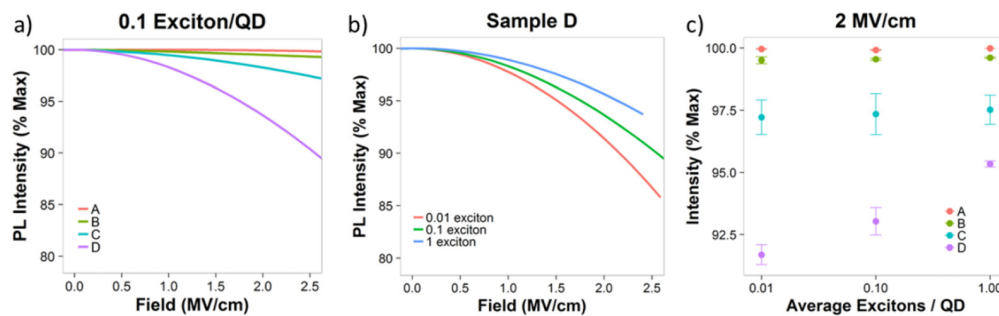


Fig. 3. (a) Generating the same average number of excitons per QD in the different samples confirms the trend shown in Fig. 2 that increasing the shell thickness increase the susceptibility to changing PL with increasing electric fields. (b) In a given sample, here D, the relative decrease in PL intensity is greater when, on average, fewer excitons are generated per QD. (c) At a given field strength, the greatest deviation in PL intensity occurs at lower numbers of excitons per QD in Sample D. In the other samples, the signal/noise ratio obscures any trend.

The origin of this phenomenon may lie in the screening of the electric field by other QDs. In our earlier work, we speculated that ionization may have accounted for the PL attenuation that were observed. The thickest-shelled sample, D, which exhibits the greatest decrease in PL intensity in response to an applied electric field, could as a result of this increased ionization be screening other QDs from the effects of the field. This phenomenon would be expected to increase with increasing illumination intensity, thus mitigating the effects of the electric field by rendering it less “felt” and resulting in the decreased PL suppression that we observe as a function of the number of excitons generated in the ensemble. The data from sample D thus suggest that QD ionization significantly screens the electric field. In the less ionized samples that experience less PL attenuation from the electric field, the effect would be less prominent; indeed we see no measureable difference among the other samples. A theoretical foundation for this concept comes from work by Marshall and Schnitzer, who predicted the screening effects of the cell’s plasma membrane on the electric field susceptibility of QDs [47]. For all of these data, it should also be noted that although the percent change in PL was greater at lower intensities for sample D, this does not necessarily correlate to the absolute change in PL intensity. In order to compensate for differences in brightness among the samples and to offer a head-to-head comparison at different excitation intensities, all the emission data were normalized.

#### 4. Conclusions

Because of the small size of cells and, in particular, the space between the phospholipid heads in the plasma membrane lipid bilayer (~5-6 nm) [44], successful use of QDs in imaging action potentials in neurons and other electrically active cells will require bright QDs that exhibit substantial changes in their PL response to electric fields. Optimizing that sensitivity by tweaking relevant properties is an important step towards developing materials for use *in vitro* and eventually *in vivo*. These include not only variables related directly to electric field susceptibility such as material composition (band structure, ionizability, etc.), shell thickness, and particle size but also factors that pertain to how the QDs might interact with a cell such as surface coating optimization for cell membrane interfacing. The results presented here demonstrate that increasing the shell thickness on a CdSe/CdS core/shell QD can improve PL sensitivity over the same core with a thinner shell by up to an order of magnitude or more. These results point to critical criteria that need to be considered in the rational design of voltage-sensitive QDs and the exciting possibility of integrating these materials into live cells, tissues, and animal systems to achieve real-time imaging capabilities heretofore not possible.

#### Appendix 1.1 QD synthesis

**Chemicals.** Selenium (Se; 99.99%), tri-*n*-octylphosphine (TOP; min. 97%), cadmium acetylacetonate, sulfur and cadmium oxide (CdO) were purchased from Strem Chemicals. *n*-Tetradecylphosphonic acid was purchased from PCI Synthesis. Hexadecylamine (HDA; technical grade, 90%), oleylamine (technical grade, 70%), *n*-octanethiol, oleic acid (technical grade, 90%) were purchased from Sigma Aldrich. 1-Octadecene (ODE; technical grade, 90%) was purchased from Acros Organics. 1-Dodecylphosphonic acid was purchased from Alfa Aesar. All the other chemicals including solvents were purchased from Sigma-Aldrich or Acros Organics and used as received.

**Preparation of CdS shell precursors.** A 0.2 M Cd oleate solution was prepared as follows: CdO (1.284 g, 10 mmol), oleic acid (12.69 mL, 40 mmol) and ODE (29.45 mL) were loaded into a 100-mL three-neck round bottom flask. The mixture was heated to 240 °C under N<sub>2</sub> to dissolve CdO and then cooled to 70 °C. After oleylamine (6.58 mL, 20 mmol) was added, the mixture was degassed under vacuum at 100 °C for 30 min, backfilled with N<sub>2</sub>, and cooled to room temperature.

**CdSe core synthesis.** Se (0.33 g, 4.2 mmol) was mixed with 4.0 mL of TOP in a 20-mL vial, which was sealed with a septum. The mixture was degassed under vacuum at 80 °C for

10 min, filled with N<sub>2</sub>, and stirred until Se was dissolved. Cadmium acetylacetonate (0.311 g, 1.0 mmol), *n*-tetradecylphosphonic acid (0.585 g, 2.1 mmol), TOP (10 mL), and HDA (5.0 g) were loaded into a 50-mL three-neck round-bottom flask. The reaction mixture was degassed under vacuum at 100 °C for 30 min. After backfilling with N<sub>2</sub>, the reaction mixture was heated to 310 °C with a heating mantle to dissolve the cadmium precursor. The heating mantle was removed, and the TOP:Se solution was swiftly injected at 310 °C with vigorous stirring. The reaction mixture was spontaneously cooled to 80 °C and annealed overnight. After cooling to 60 °C, *n*-butanol (10 mL) was added to prevent solidification of the reaction mixture. The reaction mixture was aliquoted to 40-mL vials. Excess acetone was added to each vial to flocculate the QDs. The mixtures were centrifuged at 3,800 rpm for 5 min. The supernatant was discarded, and the QD pellets were dissolved in a minimum amount of toluene. This cleaning procedure was repeated one more time. The final CdSe QD concentration was estimated following the literature method.<sup>1</sup>

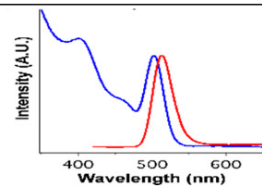
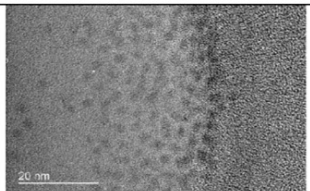
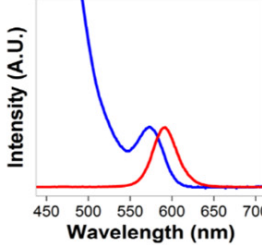
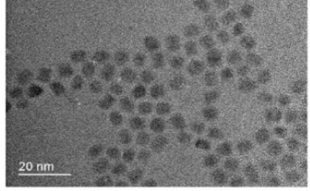
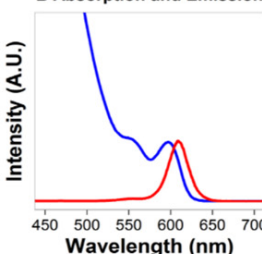
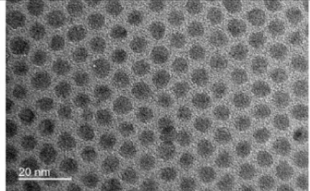
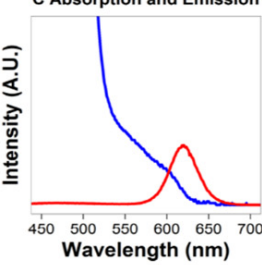
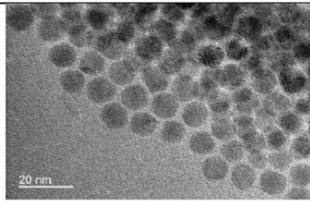
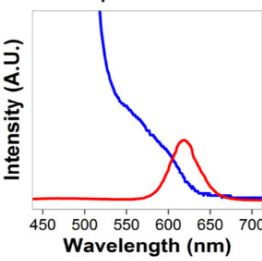
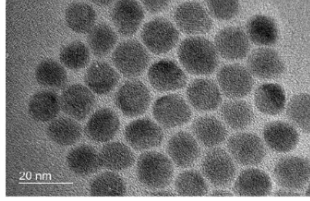
**CdSe/CdS with thin CdS shells.** ODE (5.0 mL), oleylamine (8.0 mL), TOP (5.0 mL), 1-dodecylphosphonic acid (30.6 mg,  $1.2 \times 10^{-4}$  mol), and the CdSe QD core (0.20 μmol in 4.6 mL of toluene solution) were loaded into a 100-mL four-neck round-bottom flask. The reaction mixture was degassed under vacuum at 100 °C to remove toluene and other volatiles and filled with N<sub>2</sub>. The amount of shell precursors used for the overcoating was calculated following the literature procedure [48]. For coating of the first layer of CdS, 0.2 M Cd oleate solution was added dropwise starting at 100 °C. During the Cd precursor addition, the reaction mixture was heated to 180 °C for 30 min. 0.4 M (TMS)<sub>2</sub>S in TOP was subsequently added dropwise, and the reaction mixture was kept at 180 °C for 30 min. The second CdS layer was coated in a similar fashion at 200 °C.

**CdSe with thicker CdS shells.** A typical procedure for CdSe QD cores coated with thicker CdS shells is as follows: ODE (2.0 mL), oleylamine (3.0 mL), TOP (3.0 mL), and the CdSe QD core (0.10 μmol in 2.39 mL of toluene solution) were loaded into a 100-mL four-neck round-bottom flask. The reaction mixture was degassed under vacuum at 100 °C to remove toluene and other volatiles, and filled with N<sub>2</sub>. The amount of shell precursors used for the overcoating was calculated following the literature procedure.<sup>2</sup> For coating of the first layer of CdS, 0.2 M Cd oleate solution was added to the reaction mixture at 100 °C. Then the reaction mixture was heated to 180 °C. After 30 min, 0.1 M sulfur in ODE was added dropwise, and the reaction mixture was heated to 200 °C for 45 min. The second CdS layer was coated in a similar fashion at 210 °C. From the third layer, 0.2 M Cd oleate and 0.2 M *n*-octanethiol in ODE were separately added dropwise starting at 210 °C. During the precursor addition, the reaction mixture was heated to 290 °C. 1.3-fold excess of *n*-octanethiol to Cd oleate was used during the overcoating. After the precursor addition was done, the reaction mixture was cooled.



## Appendix 1.2 Characterization of QDs

Table 1. Physicochemical characterization of QDs used in this study

Sample	Diameter from TEM (nm)	Q.Y.	Spectra (Absorption: Blue, Emission: Red)	TEM image
Core	$3.0 \pm 0.35$	0.21		
A	$5.5 \pm 0.84$	0.25	<b>A Absorption and Emission</b> 	
B	$7.4 \pm 0.47$	0.57	<b>B Absorption and Emission</b> 	
C	$10.0 \pm 0.69$	0.56	<b>C Absorption and Emission</b> 	
D	$12.8 \pm 1.46$	0.54	<b>D Absorption and Emission</b> 	

### Appendix 1.3 Device fabrication

The QDs were integrated into a Sawyer-Tower circuit through the fabrication of a device that isolated the QDs from exogenous charge. Glass substrates with a pre-patterned ITO electrode (80 nm thick, Colorado Concepts Coatings, Longmont, Co) were sonicated in acetone and rinsed with isopropanol, followed by use of an ozone asher to ensure a clean surface. After protecting a region of the ITO electrode for electrical contact using Kapton tape, an 80 nm layer of poly(vinyl pyrrolidone) (PVP) was spin coated from a 1% by weight solution of PVP in 1-butanol at 2000 rpm for 45 s. QDs at concentrations of roughly 1  $\mu\text{M}$  in a 1% poly(methyl methacrylate) (PMMA) in toluene matrix were spin-coated (45 s at 2000 rpm) onto the PVP layer, giving an 80 nm film. A second layer of PVP was spin-coated over the QD-loaded matrix using the same parameters as the first layer. Because PVP is insoluble in toluene, and PMMA is insoluble in 1-butanol, the result is a discrete, continuous PVP/PMMA\*QD/PVP tri-layer stack (confirmed via focused ion beam milling/SEM cross sectional analysis) that is electrically insulating even in electric fields in excess of 3 MV/cm. The thickness of the polymer layers was confirmed by ellipsometry. A shadow mask was then applied, and 4 nm Ti and 150 nm of Au were deposited (at 0.1 nm/s and 0.2 nm/s, respectively) using a Temescal electron beam evaporator. The active area of the completed device measured 2 mm by 2 mm.

### Appendix 1.4 Calculation of electric field on QD layer

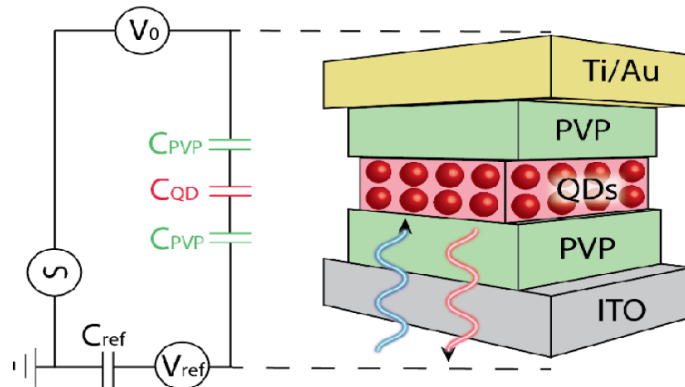


Fig. 4. Schematic of the optoelectronic device used in these studies. The QDs were dispersed in poly(methyl methacrylate) and spin-coated between layers of poly(vinyl pyrrolidone) (PVP). This dielectric sandwich was spin-coated over a transparent ITO electrode on a glass substrate and a Ti/Au electrode was deposited on top.

Table 2. Definition of variables

Definition of variables:

$V_0$	Applied potential; measured
$V_{ref}$	Potential before the reference capacitor; measured
$V_{QD}$	Potential across the QD/PMMA layer; calculated (derived below)
$C_{PVP}$	Capacitance of the PVP layer; calculated based on thickness (80 nm)
$C_{QD}$	Capacitance of the QD/PMMA layer, calculated
$C_{ref}$	Capacitance of reference capacitor, measured
$E$	Electric field across the QD/PMMA layer, calculated (derived below)
$d$	Thickness of QD/PMMA layer, measured

$$\text{Because the circuit goes to ground} \quad 0 = V_0 - V_{PVP} - V_{QD} - V_{PVP} - V_{ref}.$$

$$\text{Rearranging,} \quad V_{QD} = V_0 - 2V_{PVP} - V_{ref}.$$

$$\text{Since } V = \frac{Q}{C}, \quad V_{QD} = V_0 - 2\frac{Q_{PVP}}{C_{PVP}} - V_{ref}.$$

$$\text{Because the capacitors are in series,} \quad V_{QD} = V_0 - 2\frac{V_{ref}C_{ref}}{C_{PVP}} - V_{ref}.$$

$Q_{ox} = Q_{ref} = V_{ref}C_{ref}$ . Substituting,

$$\text{Rearranging,} \quad V_{QD} = V_0 - V_{ref} \left( 2\frac{C_{ref}}{C_{PVP}} + 1 \right).$$

$$\text{Since } E = -\frac{\Delta V}{d}, \quad E = \frac{1}{d} \left[ V_{ref} \left( 2\frac{C_{ref}}{C_{PVP}} + 1 \right) - V_0 \right].$$

The potentials  $V_0$  and  $V_{ref}$  were measured using an oscilloscope during data collection. From these values and previously measured capacitance  $C_{ref}$  and calculated  $C_{ox}$ , the voltage drop across the QD/PMMA layer was determined using the relationship  $V_{QD} = V_0 - V_{ref} \left( 2\frac{C_{ref}}{C_{PVP}} + 1 \right)$ . Knowing the thickness of the QD/PMMA film from focused ion beam lithography measurements, the strength of the electric field could be calculated.